

The New LLM Bottleneck: A Systems Perspective on Latent Attention and Mixture-of-Experts

Sungmin Yun[†], Seonyong Park[†], Hwayong Nam[†], Younjoo Lee[†], Gunjun Lee[†], Kwanhee Kyung[†], Sangpyo Kim[†], Nam Sung Kim[‡], Jongmin Kim[†], Hyungyo Kim[‡], Juhwan Cho[†], Seungmin Baek[†], Jung Ho Ahn[†]

[†]Seoul National University, Seoul, South Korea,

[‡]University of Illinois at Urbana-Champaign, Champaign, Illinois, USA

{sungmin.yun, seonyong.park, nhy4916, younjoo0614, kevin970401, kwanhee5, vnb987, jongmin.kim, jfcho2, qortmdalss, gajh}@snu.ac.kr

{hyungyo2, nskim}@illinois.edu

Abstract—Computational workloads composing traditional Transformer models are starkly bifurcated. Multi-Head Attention (MHA) is memory-bound, with low arithmetic intensity, while feedforward layers are compute-bound. This dichotomy has long motivated research into specialized hardware to mitigate the MHA bottleneck.

This paper argues that recent architectural shifts, namely Multi-head Latent Attention (MLA) and Mixture-of-Experts (MoE), challenge the premise of specialized attention hardware. We make two key observations. First, the arithmetic intensity of MLA is over two orders of magnitude greater than that of MHA, shifting it close to a compute-bound regime well-suited for modern accelerators like GPUs. Second, by distributing MoE experts across a pool of accelerators, their arithmetic intensity can be tuned through batching to match that of the dense layers, creating a more balanced computational profile.

These findings reveal a diminishing need for specialized attention hardware. The central challenge for next-generation Transformers is no longer accelerating a single memory-bound layer. Instead, the focus must shift to designing balanced systems with sufficient compute, memory capacity, memory bandwidth, and high-bandwidth interconnects to manage the diverse demands of large-scale models.

I. INTRODUCTION

Transformer-based large language models (LLMs) [52] have achieved remarkable accuracy across a variety of natural language processing tasks [11]. An LLM summarizes/prefills an input (*i.e.*, a sequence of tokens); then, it generates an output token once per decode step. A conventional LLM consists of a sequence of decoder blocks, each comprising a Multi-Head Attention (MHA) block and a Feedforward Network block. To improve scalability and efficiency, recent architectures have incorporated optimizations such as Multi-head Latent Attention (MLA) [11], which first appears at DeepSeek-V3 [27] and reduces the memory footprint of attention, and Mixture-of-Experts (MoE) [9], [15], [22], [29], [55], which enhances model capacity without a proportionally rise in compute cost by activating only a subset of experts per token [47].

Maximizing accelerator utilization when serving these models is critical for improving throughput and end-to-end latency [1]. Serving LLMs in production requires deploying systems that integrate hundreds or even thousands of accelerators (*e.g.*, GPUs [33] and TPUs [50]) to handle high query volumes

and large models [4], [41]. Inefficient utilization results in compute resources remaining idle, higher infrastructure costs, and failure to meet service-level objectives (SLOs) [59].

A key factor in serving LLMs efficiently is arithmetic intensity (*a.i.*), the ratio of arithmetic operations to memory access, measured in operations per byte (Op/B). The ridge point of an accelerator, a concept from the roofline model [54], defines the *a.i.* at which performance transitions from being *memory-bound* to *compute-bound*. To fully exploit an accelerator’s capabilities, the *a.i.* of each model layer should be configured to approach this ridge point.

In this paper, we argue that MLA and MoE fundamentally reshape the computational landscape of LLM inference. Crucially, both techniques significantly reduce per-request memory demands, especially in the decode stage, thereby enabling much larger batch sizes during inference. By introducing a latent space to attention, MLA significantly reduces the KV\$ size, which is a major bottleneck in conventional LLMs using MHA. Small KV\$ size enables much larger bath sizes in the decode stage without exceeding the memory capacity of the accelerators. Furthermore, by applying layer reordering, the *a.i.* of core attention in MLA is shifted toward the ridge point of modern accelerators while reducing memory access, enabling significantly higher throughput with large batch sizes while still satisfying service-level objectives (SLOs).

Mixture-of-Experts (MoE) enhances LLM scalability by sparsely activating a subset of experts for each token, enabling larger model capacity without proportional increases in computation. When combined with the increased batch sizes enabled by MLA, MoE can achieves *a.i.* near to the ridge point of the acceleratos in its expert FC layers with huge batch sizes. We analyze the required batch size to match the Op/B of FC layers in MoE blocks, also attention blocks, while considering the two primary factors, the memory capacity and SLO, which limiting the batch size.

Finally, we present an end-to-end analysis of LLM serving that synthesizes the insights from MLA and MoE. We demonstrate how these architectural innovations synergistically increase the feasible batch size, allowing the system to operate near the accelerator’s ridge point. Furthermore, we highlight

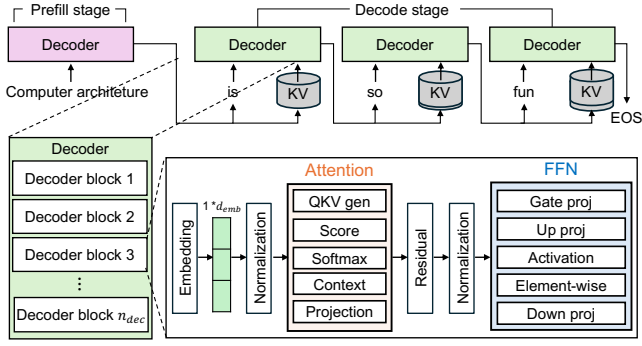


Fig. 1. Transformer-decoder-based LLM architecture.

the critical role of high-bandwidth interconnects in mitigating communication overheads across accelerators. Our evaluation shows that high bandwidth interconnects, such as NVLink, are essential for minimizing latency in expert dispatch and aggregation, enabling systems to meet service-level objectives (SLOs) with fewer devices. Together, these insights offer a guideline for designing high-throughput, low-latency LLM serving systems.

The key contributions of this paper are as follows:

- We show that layer reordering in MLA increases the arithmetic intensity of core attention, enabling large batch sizes and higher throughput near the accelerator’s ridge point.
- We analyze MoE execution and identify the batch size required to match the Op/B of expert FC layers, considering memory and latency constraints.
- We present an end-to-end analysis of LLM serving systems, highlighting how MLA, MoE, and interconnect bandwidth together enable efficient, scalable inference.

II. BACKGROUND

A. Standard LLM architecture and its layers

Despite the rapid advancements in LLM algorithms [19], [30], the transformer-based architectures [52], especially the ones using decoders only [7], remain the standard backbone across most modern LLMs (Figure 1). A transformer consists of a series of n_{dec} decoder blocks. Given an input sequence of length ℓ constituting an inference (serving) request, each token (e.g., word) is embedded into a d_{emb} -dimensional hidden state, forming a hidden state matrix $\mathbf{H}_\ell \in \mathbb{R}^{\ell \times d_{\text{emb}}}$, then provided as input to the decoder. The matrix passes through a series of decoder blocks, each equipped with its own trained weight parameters, and is transformed into a single output vector.

LLM inference consists of prefill (summarization) stage and decode (generation) stage. The prefill stage processes the entire input hidden stage matrix ($\ell = L_{\text{in}}$) to generate the first output token. Subsequently, the decode stage generates the remaining tokens auto-regressively, where each step takes the single, previously generated token ($\ell = 1$) as input to produce the next one, continuing until an end-of-sequence token is generated or the output sequence reach the maximum output token.

A decoder block in a standard LLM consists of two blocks: **Multi-Head Attention** (MHA) block and **Feed-Forward Network** (FFN) block. In MHA, a hidden state matrix \mathbf{H} is first

linearly transformed (projected) into **Query** (\mathbf{Q}), **Key** (\mathbf{K}), and **Value** (\mathbf{V}) matrices by passing through fully connected (FC) layers with pre-trained weights, which are then split into n_{hd} heads. Eq. 1 shows how \mathbf{Q} , \mathbf{K} , and \mathbf{V} for each head is computed where L denotes the current sequence length, defined as the sum of the input sequence length L_{in} and the number of tokens generated so far. During auto-regressive decoding, a KV cache (KV\$) stores past K and V values to maintain contextual information without costly recomputation. Consequently, only the new K and V vectors for the current input token are computed and appended to this cache.

$$\begin{aligned} \underbrace{\mathbf{Q}_i}_{\mathbb{R}^{\ell \times \frac{d_{\text{dec}}}{n_{\text{hd}}}}} &= \underbrace{\mathbf{H}_\ell}_{\mathbb{R}^{\ell \times d_{\text{emb}}}} \cdot \underbrace{\mathbf{W}_{\mathbf{Q}_i}}_{\mathbb{R}^{d_{\text{emb}} \times \frac{d_{\text{dec}}}{n_{\text{hd}}}}} \\ \underbrace{\mathbf{X}_i}_{\mathbb{R}^{L \times \frac{d_{\text{dec}}}{n_{\text{hd}}}}} &= \underbrace{\mathbf{H}_L}_{\mathbb{R}^{L \times d_{\text{emb}}}} \cdot \underbrace{\mathbf{W}_{\mathbf{X}_i}}_{\mathbb{R}^{d_{\text{emb}} \times \frac{d_{\text{dec}}}{n_{\text{hd}}}}} \end{aligned} \quad (1)$$

for $\mathbf{X} \in \{\mathbf{K}, \mathbf{V}\}$ and $i \in [1, n_{\text{hd}}]$

Each head performs a sequence of operations, referred to as core-attention, independently. Core-attention computes score (Eq. 2), softmax, and context (Eq. 3) operations.

$$\underbrace{\mathbf{S}_i}_{\mathbb{R}^{\ell \times (L)}} = \underbrace{\mathbf{Q}_i}_{\mathbb{R}^{\ell \times \frac{d_{\text{dec}}}{n_{\text{hd}}}}} \cdot \underbrace{[\mathbf{K}_i]^T}_{\mathbb{R}^{\frac{d_{\text{dec}}}{n_{\text{hd}}} \times L}} \quad (2)$$

$$\underbrace{\mathbf{O}_i}_{\mathbb{R}^{\ell \times \frac{d_{\text{dec}}}{n_{\text{hd}}}}} = \underbrace{\text{Softmax}\left(\frac{\mathbf{S}_i}{\sqrt{d_{\text{dec}}/n_{\text{hd}}}}\right)}_{\mathbb{R}^{\ell \times L}} \cdot \underbrace{[\mathbf{V}_i]}_{\mathbb{R}^{L \times \frac{d_{\text{dec}}}{n_{\text{hd}}}}} \quad (3)$$

Lastly, MHA performs an FC layer, attention output projection, generating MHA’s output \mathbf{U} .

An FFN block in recent LLMs consists of three FC layers and one nonlinear activation. Until GPT-3 [21], most models used an FFN block with only two FC layers and one activation. However, modern LLMs typically employ three FC layers, which improves response quality at the cost of additional computation by introducing gated activation functions [46].

Rotary Positional Embedding (RoPE) [49] is common in modern LLMs to inject positional information into token generations. RoPE encodes each token’s position through a unique rotational transformation based on its position index applied to \mathbf{Q} and \mathbf{K} before the core attention layer while leaving \mathbf{V} unchanged.

For the FC layers, all requests share the same weights in LLM inference. Batching multiple requests enables the FC weight reuse, reducing memory access overhead. As memory bandwidth scales more slowly than compute capability in modern accelerators (Table I), it becomes a major bottleneck, especially in the decode stage, where GEMV operations offer limited data reuse. While the batching improves throughput, it does not reduce per-request latency, and the batch size B is bounded by SLOs [59]. Moreover, as each request maintains its own KV\$, a larger B increases memory capacity requirements, making memory capacity another key limiter for the maximum feasible value.

TABLE I
ARITHMETIC PERFORMANCE, MAIN-MEMORY BANDWIDTH AND CAPACITY OF DEEP-LEARNING ACCELERATORS

| | V100 SXM2 [31] | A100 SXM4 [32] | H200 SXM5 [34] | B200 SXM6 [36] | TPU V5P [51] | TPU V7 [50] | MI325X [3] |
|---------------------------|----------------|----------------|----------------|----------------|--------------|-------------|------------|
| BF16 performance (TFLOPS) | 125 | 312 | 989.5 | 2250 | 459 | 2307 | 1307.4 |
| Memory bandwidth (GB/s) | 900 | 2039 | 4800 | 8000 | 2765 | 7400 | 6000 |
| HBM capacity per GPU (GB) | 32 | 80 | 141 | 192 | 95 | 192 | 256 |
| Ridge point (BF16) | 138.89 | 153.02 | 206.15 | 281.25 | 166 | 320.42 | 217.9 |

B. Representative optimizations for LLM

To efficiently serve LLMs, a myriad of optimizations—spanning both algorithmic strategies and hardware-aware techniques—have been proposed in response to ever-growing demand for LLMs.

Grouped-Query Attention (GQA): During the decode stages ($\ell = 1$), the core attention of MHA performs multiple GEMVs (see Eq. 2 and Eq. 3) between the query vectors and request-specific KV\$ matrices. These layers are highly memory-bound with a fixed arithmetic intensity (*a.i.*) of 1; thus, they make poor use of the accelerator’s compute resources [8], [20].

GQA [2] mitigates this issue. In GQA, a head of KV\$ is shared by multiple Q heads, reducing the total KV\$ size by the number of queries in a group. Reusing a KV\$ across multiple heads, *a.i.* improves while deteriorating model accuracy. An extreme variant, *Multi-Query Attention (MQA)* [45], enforces all Q heads to share a single KV head. However, due to the significant degradation in service quality observed with MQA compared to MHA and GQA, we will not discuss it further.

Multi-head Latent Attention (MLA): Even with GQA, the *a.i.* of the core attention (determined by the number of queries per group) remains around eight, and the memory capacity required for KV\$ continues to constrain the maximum feasible batch size, thereby limiting the potential benefits from batching. MLA [27] further reduces these KV\$ capacity requirements by applying a low-rank joint compression to \mathbf{Q} , \mathbf{K} , and \mathbf{V} . It first compresses a hidden state matrix into a latent space (labeled ③ in Figure 2) to form a compressed Q (\mathbf{C}_Q) and a compressed KV (\mathbf{C}_{KV}) through projection using \mathbf{W}_{CQ} and \mathbf{W}_{CKV} (Eq. 4). Then, it decompresses them (labeled ④, ⑤ and ⑥ in Figure 2) through projections using the decompression weights \mathbf{W}_{DX_i} , where $\mathbf{X} \in \{\mathbf{Q}, \mathbf{K}, \mathbf{V}\}$, forming the full \mathbf{Q}_i , \mathbf{K}_i , and \mathbf{V}_i , which are then used to perform the same core attention as in a standard MHA block (Eq. 5 and Eq. 6).

$$\underbrace{\mathbf{C}_Q}_{\mathbb{R}^{\ell \times d_{Qco}}} = \mathbf{H}_L \cdot \underbrace{\mathbf{W}_{CQ}}_{\mathbb{R}^{d_{emb} \times d_{Qco}}}, \quad \underbrace{\mathbf{C}_{KV}}_{\mathbb{R}^{L \times d_{KVco}}} = \mathbf{H}_L \cdot \underbrace{\mathbf{W}_{CKV}}_{\mathbb{R}^{d_{emb} \times d_{KVco}}} \quad (4)$$

$$\mathbf{S}_i = \mathbf{Q}_i \cdot (\mathbf{K}_i)^T = \underbrace{(\mathbf{C}_Q \cdot \mathbf{W}_{DQ_i})}_{\mathbb{R}^{\ell \times \frac{d_{dec}}{n_{hd}}}} \cdot \underbrace{(\mathbf{C}_{KV} \cdot \mathbf{W}_{DK_i})^T}_{\mathbb{R}^{L \times d_{KVco}} \times \frac{d_{dec}}{n_{hd}}} \quad (5)$$

$$\mathbf{O}_i = \text{Softmax}\left(\frac{\mathbf{S}_i}{\sqrt{d_{dec}/n_{hd}}}\right) \cdot \underbrace{(\mathbf{C}_{KV} \cdot \mathbf{W}_{DV_i})}_{\mathbb{R}^{d_{KVco}} \times \frac{d_{dec}}{n_{hd}}} \quad (6)$$

Notably, instead of retaining the separate n_{hd} heads of key and value tensors, $\mathbf{K}_i, \mathbf{V}_i \in \mathbb{R}^{L \times \frac{d_{dec}}{n_{hd}}}$, MLA stores a single latent KV\$, $\mathbf{C}_{KV} \in \mathbb{R}^{L \times d_{KVco}}$. It is then used to reconstruct both the key and value heads. As the latent KV\$ dimension d_{KVco} is

much (usually more than an order of magnitude) smaller than both d_{emb} and d_{dec} , it significantly reduces memory usage (by a factor of $\frac{2d_{dec}}{d_{KVco}} = 64$ for DeepSeek-R1) and decreases data movement during the core-attention. However, these gains come at the cost of additional overhead for on-demand KV decompression *per decode stage*.

One of MLA’s key features is the decoupling of RoPE. Instead of directly applying RoPE on Q and K, RoPE is separately computed and added element-wise in the score layer (labeled ⑥ in Figure 2). With the removal of the nonlinear layer between the QKV generation layer and core-attention, Eq. 5 can be algebraically rewritten (see Eq. 7) to enable *reordering* [27],¹ an optimization that improves data reuse by rearranging the layers in the attention block.

$$\begin{aligned} \mathbf{S}_i &= \mathbf{Q}_i \cdot (\mathbf{C}_{KV} \cdot \mathbf{W}_{DK_i})^T \\ &= \mathbf{Q}_i \cdot (\mathbf{W}_{DK_i}^T \cdot \mathbf{C}_{KV}^T) \\ &= (\mathbf{Q}_i \cdot \mathbf{W}_{DK_i}^T) \cdot \mathbf{C}_{KV}^T \\ \mathbf{S} &= \begin{bmatrix} \mathbf{Q}_1 \cdot \mathbf{W}_{DK_1}^T \\ \mathbf{Q}_2 \cdot \mathbf{W}_{DK_2}^T \\ \vdots \\ \mathbf{Q}_{n_{hd}} \cdot \mathbf{W}_{DK_{n_{hd}}}^T \end{bmatrix} \cdot \mathbf{C}_{KV}^T \end{aligned} \quad (7)$$

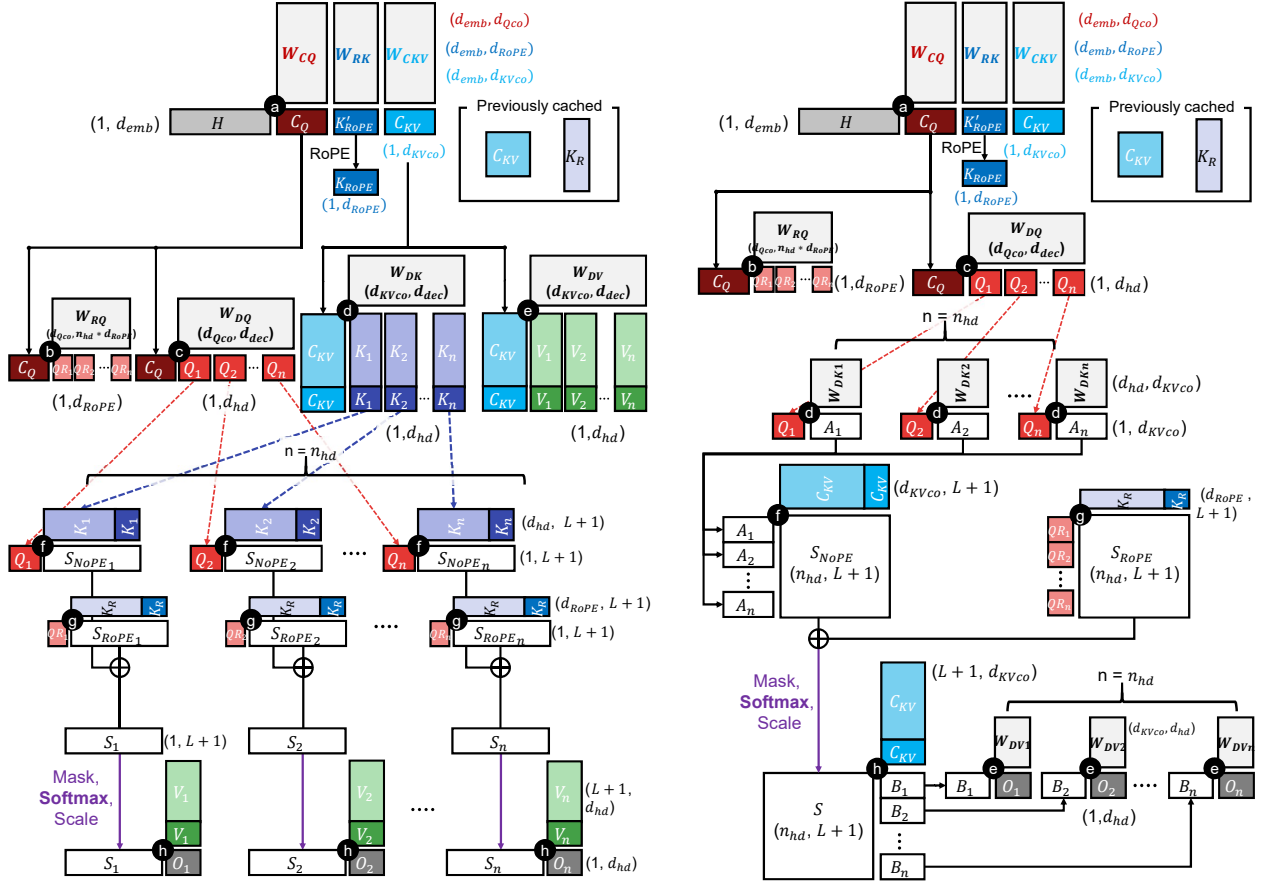
A similar reordering can also be applied to the context layer:

$$\begin{aligned} \mathbf{O}_i &= \text{Softmax}\left(\frac{\mathbf{S}_i}{\sqrt{d_{dec}/n_{hd}}}\right) \cdot (\mathbf{C}_{KV} \cdot \mathbf{W}_{DV_i}) \\ &= \left(\text{Softmax}\left(\frac{\mathbf{S}_i}{\sqrt{d_{dec}/n_{hd}}}\right) \cdot \mathbf{C}_{KV}\right) \cdot \mathbf{W}_{DV_i} \end{aligned} \quad (8)$$

The reordering transforms the score and context layers from GEMV to GEMM operations without affecting their results. Combined with the use of latent space, this reordering synergistically improves the *a.i.* and reduces the memory accesses of core-attention (further elaborated in §V).

Mixture of Experts (MoE): Although a common belief is that larger models with more parameters produce higher-quality responses [24], the substantial computational overhead associated with scaling LLMs hinders their adoption. MoE [15] addresses this issue by employing sparse activation in FFN blocks called an *expert*. MoE introduces a pool of experts and activates only a small subset of these experts for each input. In particular, recent LLMs [11], [12], [29] adopt a hybrid architecture consisting of two types of experts: a *shared expert*

¹Although the DeepSeek papers [12], [27] refer to this technique as “Absorption,” we use the term “decompression matrix multiplication reordering” or simply “reordering,” to distinguish it from weight fusion, which merges multiple weight matrices into a single computational step.



(a) MLA computational flow without reordering

(b) MLA computational flow with reordering

Fig. 2. Computation flow of multi-head latent attention (MLA) with/without layer reordering. ① to ⑩ refer to the layers of MLA (e.g., ①: QKV compression, ②: Q RoPE, ③: Q decompression, ④: K decompression, ⑤: V decompression, ⑥: score, ⑦: K RoPE, ⑧: context).

and *routed experts*. The former is activated for every token during inference, whereas the latter are selectively activated based on a routing mechanism that dynamically assigns n_k experts out of n_e experts to each token. The computational procedure of an MoE block can be described as

$$\text{Router}(\mathbf{u}) = \mathbf{E} \in \{1, 2, \dots, n_e\}, |\mathbf{E}| = n_k < n_e$$

$$\text{MoE}(\mathbf{u}) = \left(\sum_{e \in \mathbf{E}} \text{Expert}_e(\mathbf{u}) \right) + \text{Expert}_{\text{shared}}(\mathbf{u}) \quad (9)$$

By utilizing only n_k experts ($n_k < n_e$), along with one shared expert per token at runtime, MoE scales the model with significantly lower computational overhead. The values of n_k and n_e vary across different models: DeepSeek-R1 [11] employs eight routed experts selected from a pool of 256, while Llama 4 Maverick [29] uses a single routed expert selected from a pool of 128.

C. Hardware efficiency & arithmetic intensity (a.i.)

When serving LLMs, three key factors determine service latency and throughput: *arithmetic performance*, *memory bandwidth*, and *memory capacity* of an accelerator. High arithmetic performance enables fast execution of compute-intensive layers, such as GEMMs on large tensors during the prefill stage (e.g., Eq. 1). To fully leverage this arithmetic capability,

sufficient memory bandwidth is essential to quickly supply the data required for these computations. Such high bandwidth can only be fully utilized when the memory capacity is large enough to accommodate the entire working set; otherwise, data must be fetched from lower-bandwidth sources (e.g., via a PCIe link), severely limiting performance.

a.i. is a useful metric for evaluating the expected performance of an algorithm with ample parallelism on a given accelerator. It is the ratio of operations performed to the amount of data accessed from memory in bytes (Op/B) during execution. The *ridge point* of an accelerator (RP_{acc}) [54] refers to the Op/B at which performance shifts from memory-bound to compute-bound. It is calculated as the ratio of peak arithmetic throughput to peak memory bandwidth of the accelerator. If the *a.i.* of a compute block is lower than the ridge point, memory bandwidth becomes the primary bottleneck; its execution time is largely determined by $\frac{\text{memory access}}{\text{memory bandwidth}}$. By contrast, an Op/B value higher than the ridge point indicates that a sufficient number of operations are performed per unit of data, making the block compute-bound, allowing the accelerator's arithmetic throughput to saturate. Then, the execution time would be bounded by $\frac{\# \text{ of operations}}{\text{arithmetic throughput}}$ [54].

D. LLM serving systems

LLMs have progressively scaled up in size to improve quality, their computation and memory demands now far exceed the capacity of a single accelerator. For example, DeepSeek-R1 requires over 1250 GB of memory with BF16 precision, far exceeding the main memory capacity of the latest accelerators (*e.g.*, 192 GB per NVIDIA B200 GPU, see Table I). Even with sufficient memory capacity, limited compute resources may still lead to unacceptable latency or low throughput. Thus, LLM serving systems have evolved to utilize multiple accelerator instances.

In LLM serving systems, various parallelisms are employed to efficiently distribute the model weights and computations across accelerators [6], [14]. The most prominent approaches include data parallelism (*DP*), tensor parallelism (*TP*) [48], and expert parallelism (*EP*) [15], [43]. *DP* replicates the model weights across multiple accelerators and splits the input batch into sub-batches, processing each sub-batch independently on a separate accelerator without inter-accelerator communication. However, it introduces memory inefficiency as identical model weights are stored repeatedly on each accelerator.

TP partitions activation, weights, or both between accelerators, allowing each to compute partial results of a single operation in parallel. It improves the utilization of memory and compute resources, but introduces inter-accelerator communication as partial results must be exchanged and aggregated during execution.

EP distributes experts in MoE blocks evenly across accelerators. The output vector of an attention block is dispatched to the appropriate accelerators that store the routed experts. After the corresponding MoE blocks have been computed, the results in different accelerators are combined. This dispatching and combining incur additional communication overhead. deg_{TP} , deg_{DP} , and deg_{EP} denote the degree of *TP*, *DP*, and *EP*, respectively. Moreover, different types of parallelism can be applied selectively at the block level, enabling optimization based on the computational characteristics of each block.

Pipeline parallelism (*PP*), an inter-layer model parallelization technique, partitions sequential layers into multiple accelerators to address memory capacity limitations with lower communication cost over *TP*. However, *TP* is often preferred over *PP* in LLM inference as it directly reduces the latency of computations, whereas *PP* can not. Another core weakness of *PP* is the creation of inevitable bubbles, where accelerators sit idle as they have to wait for the input data from the previous layer computed by other accelerators in the pipeline. Although it can be mitigated by processing several micro-batches to keep the pipeline full, this method’s effectiveness diminishes with smaller batch sizes, leading to hardware under-utilization. Thus, in this paper, we focus on *TP* rather than *PP*.

As the LLM serving system gets bigger, interconnection becomes a critical factor in determining system performance and scalability. Efficient interconnect bandwidth topology directly impacts the cost and latency of communication between accelerators [10], [12], [35].

TABLE II

SYMBOLS USED THROUGHOUT THIS PAPER, THEIR DESCRIPTIONS, AND THE EXEMPLAR PARAMETERS USED IN DEEPSEEK-R1 [11]

| Term | Description | DeepSeek-R1 |
|---------------------|---|-------------|
| d_{emb} | Embedding dimension (dim) | 7168 |
| n_{hd} | Number of heads | 128 |
| d_{hd} | Head dim | 128 |
| d_{dec} | Decompressed Q, K, V dim ($= n_{hd} \times d_{hd}$) | 16384 |
| d_{Qco}, d_{KVco} | Compressed Q, KV dim | 1536, 512 |
| d_{RoPE} | Rotary PE dim | 64 |
| d_{MoE} | MoE intermediate dim | 2048 |
| n_e | Number of routed experts | 256 |
| n_k | Number of routed experts per token | 8 |

III. EXPERIMENTAL SETUP

To evaluate LLM serving performance in various configurations, we built an in-house simulator based on the LLMsimulator [44], which was used in [56]. Our in-house simulator is configured to model the latest NVIDIA B200 GPU, whose key parameters are specified in Table I. By default, we assume all GPUs in a group are fully connected via NVLink fifth generation, providing 900GB/s of unidirectional bandwidth following the NVL72 system topology [33]. For each experiment, we specify the number of GPUs per group and note when InfiniBand XDR (100 GB/s) is used for inter-group communication. All experiments used DeepSeek-R1 (key parameters summarized in Table II and specified in Table IV) with BF16 data size for all parameters, KV\$, and activations. Following [16], [35], [40], [59], the system is *disaggregated*, with the prefill and decode stages executed on separate machines.

We also varied the batch size by stage. In the decode stage, where a single vector is processed for each request, batching is crucial for achieving high hardware utilization, while the prefill stage derives less benefit from batching as it already processes a large sequence of tokens, which can effectively saturate the compute resources [1], [13], [59]. Since the decode stage dominates overall execution time [39], our analysis primarily focuses on the decode stage.

IV. DEMYSTIFYING THE COMPOUND INTERPLAY OF ALGORITHM–HARDWARE–PARALLELISM

A. The latest LLM wears MLA and MoE

Contemporary LLMs, leveraging MLA and MoE, demonstrate significant enhancements in both inference latency and throughput. Figure 3 illustrates this by comparing the time per output token (TPOT) and token generation throughput between DeepSeek-R1 and GPT-3 during inference on a 32 B200 GPU system. Hereafter, the blurred area indicates configurations where out-of-memory errors occurred. This comparison reveals an impressive throughput improvement of up to $53.67\times$, alongside a notable increase in the maximum feasible batch size (B). We delve into how MLA and MoE impact the computational characteristics of primary computing blocks within LLM execution on typical multi-accelerator serving systems. Given the alterations in model structure and weight distribution across blocks, we reassess optimal serving

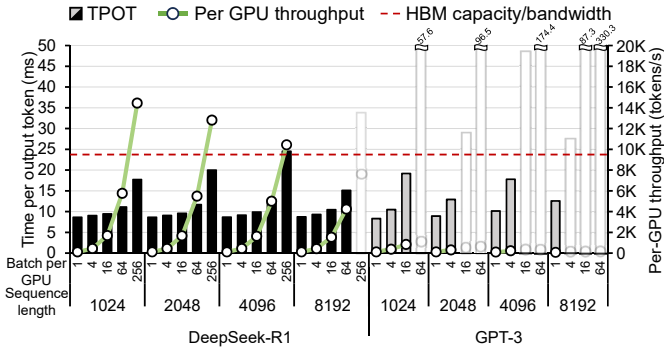


Fig. 3. Time per output token and per-device throughput of DeepSeek-R1 and GPT-3 across varying sequence length L and batch size B . The blurred area indicates configurations where out-of-memory errors occurred and the red dashed line represents the time required to read all data from HBM, which determines the maximum feasible combinations of (B, L) . The experiment assumes a 32 NVIDIA B200 GPU system.

strategies based on our observations. We especially focus on long sequences (over 1024) in this paper, following recent trends, such as chain of thought [53], [58], that keep increasing the average sequence lengths [5], [25], [38]. Our observations are highlighted in separate boxes and categorized into two types: primary (*Observation-P*) and supportive (*Observation-S*).

B. limitations of conventional LLMs

Core attention’s memory and computational demands remain consistent per request, even with batching. This is because, unlike FC layers that benefit from batching for weight memory access amortization, core attention processes activations unique to each request. Thus, its *a.i.* is not altered by batching, as mandated by the model architecture.

Observation-S1: The *a.i.* of core attention is decided by the model architecture, regardless of the batch size.

Figure 4 shows total model weight size breakdowns for a conventional LLM (GPT-3): Until FC layers batch enough requests to reach the ridge point RP_{acc} , the runtime of each layer is proportional to the memory usage, as they are all bounded by reading data from memory.

As the sequence length and batch size (B) increase, core attention becomes the main bottleneck in the decode stage, limiting throughput and leaving hardware underutilized [20], [39], [56]. The maximum feasible B in an LLM system is determined by the memory capacity that remains after storing the model parameters because the residual capacity accommodates the per-request KV\$. FC layers that use weights are in a memory-bound region when B is smaller than RP_{acc} . With an insufficient maximum B , time per output token (TPOT) is bounded by the time required to read the entire memory, leaving computing resources in an accelerator idle.

Although larger models generally translate to higher quality outputs, a dense model must touch every parameter at inference time, making the computational cost grow linearly with

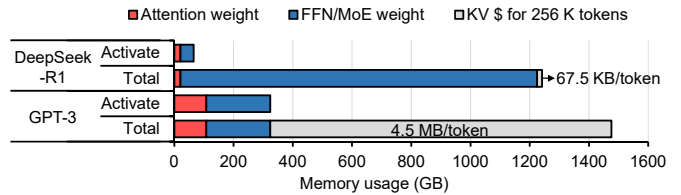


Fig. 4. Memory usage comparison of DeepSeek-R1 and GPT-3, including attention weight, FFN/MoE weight, and the KV\$ for 256K tokens with BF16 precision. While GPT-3 needs to use full model parameters during inference, DeepSeek-R1, which employs MoE architecture, activates only 37B parameters per token, requiring approximately 70GB of memory usage.

model size. Figure 4 compares the number of activated parameters per token between DeepSeek-R1, which employs a MoE network, and GPT-3 that uses a dense FFN. While the model size of GPT-3 is much smaller than that of DeepSeek-R1, the amount of computation per token didn’t scale accordingly.

C. Insights into contemporary accelerators for LLMs

An algorithm’s performance must be evaluated relative to the hardware’s ridge point. For example, in an FC layer, increasing batch size raises *a.i.* and throughput prior to reaching this point. Beyond the ridge point, the system becomes compute-bound, and batching further requests only increases latency without yielding additional throughput gains. Thus, the implications of changing an algorithm’s *a.i.* (Op/B) are meaningful when interpreted in the context of this ridge point.

The B200 GPU provides approximately $18\times$ higher arithmetic throughput compared to the V100 GPU, representing the most significant improvement among the accelerators listed in Table I. However, because both arithmetic performance and memory bandwidth scale with technology, the B200’s ridge point increases by only a modest factor of 2.02 compared to the V100. Thus, contemporary accelerators exhibit ridge points within a narrow range of 200-400 Op/B.

Observation-S2: Modern accelerators typically have the ridge points (RP_{acc}) in the range of 200 to 400 Op/B.

V. INSIGHTS ON ATTENTION

We analyze the computational characteristics of a key computation block, MLA, which is composed of multiple FC layers and a core attention.

A. Introducing latent space to attention

MLA employs low-rank joint compression to the attention block, reducing its projection weight size and the associated FC layer compute. Thus, attention block’s parameter footprint shrinks substantially both in absolute size and as a fraction of total model parameters. With this reduced weight burden, replicating its FC layer parameters across devices is far more tractable, making DP for the attention block more feasible.

A key limitation of the maximum batch size on conventional LLMs is the KV\$ size. MLA introduces latent space on attention, drastically reducing the stored KV\$ (C_{KV}) size (Figure 4). For conventional LLM, n_{hd} number of heads with d_{hd} dimensioned K and V are cached per layer. In the case

TABLE III
COMPARISON OF MLA WITH AND WITHOUT THE REORDERING IN TERMS OF FLOPS, MEMORY ACCESS, AND *a.i.* FOR PREFILL AND DECODE STAGES.

| Layer | Phase | Reordering | FLOPS | Asymptotic Memory Access | <i>a.i.</i> | <i>a.i.</i> in DeepSeek-R1 |
|---------|--------------|------------|---------------------------|---------------------------------------|--|----------------------------|
| Prefill | K decompress | without | $B2Ld_{KVco}n_{hd}d_{hd}$ | $2BLn_{hd}d_{hd}$ | $\approx d_{KVco}$ | ≈ 512 |
| | | with | $B2Ld_{KVco}n_{hd}d_{hd}$ | $2B(Ln_{hd}d_{hd} + Ln_{hd}d_{KVco})$ | $\approx (d_{hd}^{-1} + d_{KVco}^{-1})^{-1}$ | ≈ 100 |
| | Score | without | $B2n_{hd}L^2d_{hd}$ | $2Bn_{hd}L^2$ | $\approx d_{hd}$ | ≈ 128 |
| | | with | $B2n_{hd}L^2d_{KVco}$ | $2Bn_{hd}L^2$ | $\approx d_{KVco}$ | ≈ 512 |
| Decode | K decompress | without | $B2d_{KVco}Ln_{hd}d_{hd}$ | $2BLn_{hd}d_{hd}$ | $\approx d_{KVco}$ | ≈ 512 |
| | | with | $B2d_{KVco}n_{hd}d_{hd}$ | $2Bd_{KVco}n_{hd}$ | $\approx d_{hd}$ | ≈ 128 |
| | Score | without | $B2n_{hd}Ld_{hd}$ | $2Bn_{hd}d_{hd}L$ | ≈ 1 | ≈ 1 |
| | | with | $B2n_{hd}Ld_{KVco}$ | $2B(d_{KVco}L + n_{hd}L)$ | $\approx (d_{hd}^{-1} + d_{KVco}^{-1})^{-1}$ | ≈ 100 |

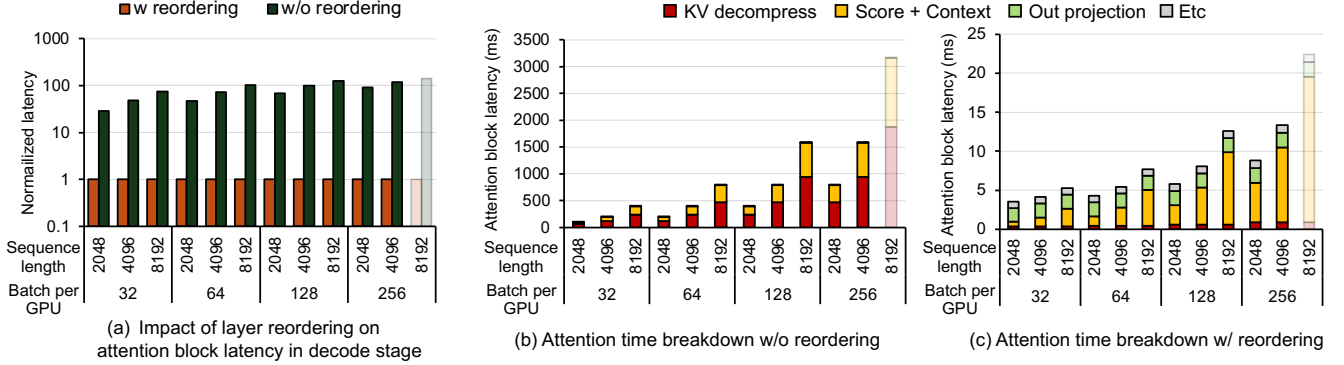


Fig. 5. (a) Normalized latency of the attention block in the decode stage without reordering compared to a reordered Attention block. (b) and (c) shows execution time ratio of each layer in the attention block in the decode stage with and without reordering, across varying sequence length L and batch size B . The experiments assume a 32 NVIDIA B200 GPU system.

of DeepSeek-R1, K and V share the same compressed cache with a dimension of $d_{KVco} + d_{RoPE}$ per layer. In GPT-3, KV\$ consumes 4.5MB ($= d_{dec} \times n_{dec} \times (K \& V) \times FP16 = 12288 \times 96 \times 2 \times 2B$) per token, whereas C_{KV} in DeepSeek-R1 requires only 67.5KB ($= (d_{KVco} + d_{RoPE}) \times n_{dec} \times BF16 = 576 \times 61 \times 2B$) per token. With reduced KV\$ size, the feasible batch size for FC layers increases to better exploit compute resources. However, like conventional LLMs, MLA has an MHA structure in the core attention, suffering from extremely low arithmetic intensity (≈ 1), and it needs C_{KV} decompression in demand on runtime.

B. Impact of Reordering MLA

The reordering explained in §II-B drastically reduces the latency of attention blocks during the decode stage, whereas it rather increases the latency during the prefill stage. It is because the reordering in MLA significantly changes computation characteristics, such as FLOPs, memory access, and *a.i.*

Table III compares the FLOPs and memory requirements of the reordered and not-reordered MLA in K decompression and score layers (d and f in Figure 2) across both prefill and decode stages when a single accelerator is used. V decompression and context layers (e and h in Figure 2) exhibit similar trends, as K and W_{DK} share the same structure with V and W_{DV} , respectively. This analysis yields several notable observations.

Without reordering, the core attention in MLA preserves the same computational flow as MHA except for the runtime compression and decompression steps immediately preceding

it. The required computation (FLOPs) and memory access for the K decompression and score layers are proportional to B and L during the decode stage (see Table III), whereas those of the FC layers do not scale with L . Thus, KV decompression and core attention dominate the execution time of an attention block as L increases (see Figure 5(b)). At $B = 256$ and $L = 4096$, KV decompression and core attention account for 59% and 40% of an attention block latency, respectively.

Observation-P1: In the decode stages of MLA without reordering, KV decompression and core attention layers dominate the runtime of MLA’s attention blocks.

After applying the layer reordering, MLA multiplies W_{DK} with Q . As the size of Q is independent of L in the decode stage, reordering substantially reduces computation in a K decompression step by a factor of L , as this layer no longer decompresses an entire C_{KV} (Table III). The portion of K decompression—previously the dominant component—has been significantly reduced due to reordering (see Figure 5(c)).

By contrast, this benefit disappears in the prefill stage as the size of Q is proportional to $L = L_{in}$, making the computational cost of K decompression unchanged. The reordering rather increases the amount of computation required for the score layer by d_{KVco}/d_{hd} (4 for DeepSeek-R1) times in both stages, as it replaces the original score layer with a multiplication between $Q_i \cdot W_{DK_i}^T$ and C_{KV}^T (see Eq. 7), where one of the matrix dimensions becomes d_{KVco} instead of d_{hd} .

Observation-P2: While the layer reordering maintains or reduces the FLOPs of KV decomposition, it instead increases the FLOPs of core attention in both stages.

With the layer reordering, core attention reads C_{KV} instead of decompressed KV\$, reducing memory access by d_{dec}/d_{KVco} . Combined with the increase of FLOPs highlighted at *Obs.P2*, the *a.i.* of both the score and context layers reaches approximately n_{hd} via head-wise batching (Ⓐ and Ⓑ in Figure 2) in the decode stages.

FlashMLA [23], a GPU-optimized implementation, further doubles this Op/B by reusing C_{KV} loaded during the score layer in the subsequent context layer. A $2n_{hd}$ Op/B (*i.e.*, 256 in DeepSeek-R1) closely approaches the ridge point of modern accelerators (*Obs.S2*). Since the *a.i.* of core attention is near RP_{acc} of modern accelerators, its performance is balanced between compute-bound and memory-bound. This means the time spent on computation is still approximately equivalent to the time spent on C_{KV} access, thereby the throughput of core attention improved approximately by $2d_{dec}/d_{KVco}$ ($= 64$ for DeepSeek-R1).

In contrast, reordering increases the latency of attention blocks during the prefill stage. In the KV decomposition layer, the FLOPs remain unchanged, while memory access increases, leading to longer execution time. For the core attention, memory access and FLOPs grow when the layer reordering is applied because its memory footprint is dominated by input/output activations of core attention, unlike the decode stages. Specifically, layer reordering expands the activation’s dimension per head from d_{hd} to d_{KVco} . Thus, the additional computation outweighs any potential gains. Applying the layer reordering deteriorates the performance of attention blocks during the prefill stage (*Obs.P2*).

Putting it all together, layer reordering significantly reduces the latency of KV decomposition and core attention within the overall attention block latency in the decode stage (see Figure 5(a)). Thus, layer reordering improves the execution time of the attention block in the decode stage by $119.07\times$, when $B=256$ and $L=4096$. When $B=1$ and $L=4096$, the attention block’s latency in the prefill stage with reordering is $2.02\times$ higher than that without reordering. Hereafter, the prefill stage uses MLA without reordering and the decode stage uses MLA with reordering.

Observation-P3: Layer reordering enhances the attention block’s throughput by substantially improving its *a.i.*, primarily by reducing memory access despite the additional computational overhead in the decode stage; however, it degrades performance in the prefill stage.

MLA diminishes the need for specialized attention hardware. In contrast to MHA or GQA, where core attention in decode stages typically shows low *a.i.* (Op/B in the 1–8 range) [56], prompting the development of processing-in-memory or near-data-processing architectures [20], [28], [39], [56] for acceleration, MLA and reordering significantly

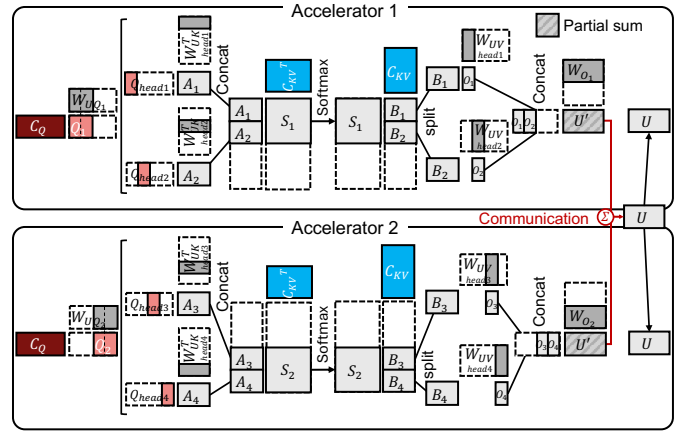


Fig. 6. Computation flow of an MLA attention block with $deg_{TP} = 2$ and $n_{hd} = 4$ on our experimental setup.

increase the Op/B of core attention, approaching RP_{acc} . Consequently, previous attention-specific hardware is less effective for accelerating MLA attention because performance is no longer constrained by memory bandwidth.

C. Parallelism on MLA

TP offers little latency benefit once reordering is applied in the attention block. Although reordering massively lowers the core attention latency, the latency still scales with B and L in the decode stage and dominates at large B and L (Figure 5(c)). When heads are independent, as in MHA, head-wise TP can distribute the KV\$ across multiple accelerators, reducing latency. Also, *a.i.* is preserved within a head as it is not affected by TP.

In the reordered MLA, all heads share the same C_{KV} ; thus, the capacity benefit from TP diminishes. As depicted in Figure 6, TP reduces the number of heads batched on each accelerator, thereby reducing the *a.i.* by deg_{TP} .

This Op/B reduction lowers per-accelerator computational throughput by around $deg_{TP}\times$, effectively canceling out the performance gain from scaling out to deg_{TP} accelerators. Figure 7 compares the latency impact of TP on a reordered and not-reordered MLA attention block. Although the FC layers in an attention block benefit from TP, the overall latency improvement is limited because the core attention takes the majority of the runtime of the attention block. Moreover, each head is multiplied by full C_{KV} , requiring all deg_{TP} accelerators to store redundant copies of C_{KV} , leading to memory inefficiency.

Observation-P4: In the decode stage with reordering, tensor parallelism fails to provide meaningful latency reduction.

VI. INSIGHTS ON MIXTURE OF EXPERTS

The execution time of MoE blocks is primarily dominated by performing experts and the communication required for dispatching and combining tokens [57]. In a multi-accelerator

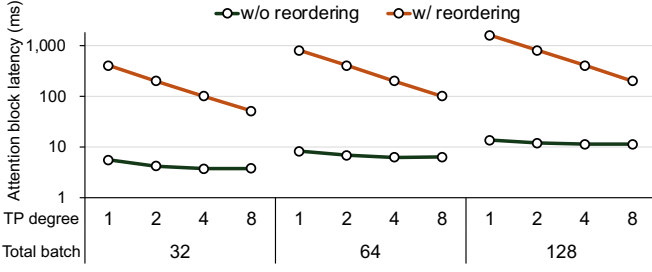


Fig. 7. Latency of the Attention block with and without reordering as batch sizes and deg_{TP} vary when $L = 4096$.

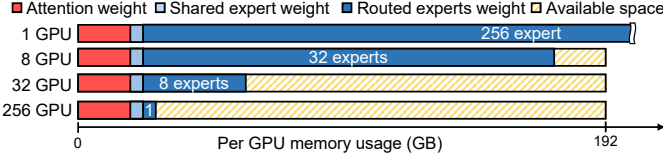


Fig. 8. Per-GPU memory usage for DeepSeek-R1 as more GPUs are used.

system, efficient expert computation requires careful design of the deployment strategy, including data distribution and parallelization, to maximize each accelerator’s arithmetic throughput by batching FC layers in each expert, while meeting accelerator memory and SLO constraints. Meanwhile, communication overhead between accelerators in serving system is highly dependent on the system-wide interconnect (e.g., NVLink [17], [36], InfiniBand [18], [37], and optical links [42]) specification. In this section, we analyze the impact of both factors on the performance of MoE blocks.

A. Maximize compute utilization in FC layers

Although both attention and MoE blocks perform FC layers, the effective batch size differs even under a fixed system-wide batch size B , due to the distinct parallelism strategies employed in each block. In the attention block, B requests are evenly distributed across deg_{DP} groups of accelerators, where each group uses TP to process $\frac{B}{\text{deg}_{\text{DP}}}$ requests in parallel. The Op/B of the FC layers in this block is around $\frac{B}{\text{deg}_{\text{DP}}}$. In contrast, the MoE block utilizes EP, which processes each expert on a single accelerator by gathering attention results from other accelerators. Thus, the effective batch size for MoE blocks remains B . Considering that each token is routed to n_k experts among n_e experts, assuming uniform selection², each expert processes $B \cdot n_k/n_e$ tokens. The average *a.i.* of MoE blocks becomes around $B \cdot n_k/n_e$. To make the FC layers in both attention and MoE blocks fully utilize target accelerators, the batch size B should satisfy:

$$\begin{aligned} B &\geq B_{\text{attn}} = \text{RP}_{\text{acc}} \cdot \text{deg}_{\text{DP}} \\ B &\geq B_{\text{MoE}} = \text{RP}_{\text{acc}} \cdot \frac{n_e}{n_k} \end{aligned} \quad (10)$$

²To avoid unbalanced expert load, SwitchTransformer [15] and GShard [26] introduce an auxiliary loss, and DeepSeek-V2 [27] incorporates a bias term to balance the routing among experts. Following these, we assume the expert load is not highly skewed and approximately follows a uniform distribution [56].

where RP_{acc} denotes accelerator’s ridge point and B_{attn} and B_{MoE} are the batch sizes that achieve RP_{acc} in *a.i.* for the FC layers of an attention and MoE block, respectively. We denote the minimum B that satisfies Eq. 10 as $B_{\text{RP}} = \max(B_{\text{attn}}, B_{\text{MoE}})$.

We observe that B_{attn} is influenced by deg_{DP} whereas B_{MoE} is not. Since n_e and n_k are model parameters, the *a.i.* of the FC layers in an MoE block is determined once B and the model are fixed. In other words, the batch size that fully utilizes the MoE block, denoted B_{MoE} , is determined solely by the model and the target accelerator’s ridge point, independently of n_{acc} and the chosen parallelism strategy.

Observation-P5: B_{MoE} is determined once the model and the target accelerator are fixed.

B. Two primary factors limiting batch size

While batching B_{RP} requests is desirable, feasible batch size is limited by two factors; memory capacity and SLO.

Memory capacity: To fully utilize the accelerator’s computational resources, data must be served at high bandwidth, which requires the entire working set to reside in the main memory (e.g., HBM) of the accelerators. This working set includes the weights for attention and MoE blocks, as well as KV\$. Since model weights are predetermined, serving systems typically use the remaining memory for activations and KV\$, whose sizes are proportional to B . Thus, the memory space requirements for model weights determine the maximum feasible batch size (B_{cap}) as follows:

$$B_{\text{cap}} = \frac{M_{\text{cap}} \cdot n_{\text{acc}} - n_{\text{dec}} \cdot (M_{\text{attn}} \cdot \text{deg}_{\text{DP}} + M_{\text{MoE}})}{n_{\text{dec}} \cdot M_{\text{KVcache}} \cdot L + M_{\text{act}}(L)} \quad (11)$$

where $M_{\text{cap}} \cdot n_{\text{acc}}$ denotes the capacity of a system composed with n_{acc} accelerators, each having M_{cap} capacity. M_{attn} and M_{MoE} represent the model weight sizes of a single decoder block’s attention and MoE, respectively. We denote the KV\$ size per token for each decoder block as M_{KVcache} . The activation memory required by a decoder block for a single token on each accelerator, M_{act} , is assumed to depend on the sequence length L . As the activation memory is reused across multiple decoder blocks, the term $M_{\text{act}}(L)$ in Eq. 11³, does not scale with n_{dec} . To batch B_{RP} requests, B_{cap} should be greater than B_{RP} .

SLO: As excessive batching of requests incurs latency overheads, SLO becomes another limiting factor for feasible batch sizes. In a disaggregated system, the time per output token (TPOT)—a key latency metric in LLM serving—is determined

³The equation assumes that all decoder blocks contain MoE layers, so the total MoE weight stored per accelerator is multiplied by n_{dec} . However, in models like DeepSeek-R1, the first three layers are not MoE layers, and thus the correct factor should be $n_{\text{dec}} - 3$. This factor may vary slightly depending on the specific model architecture.

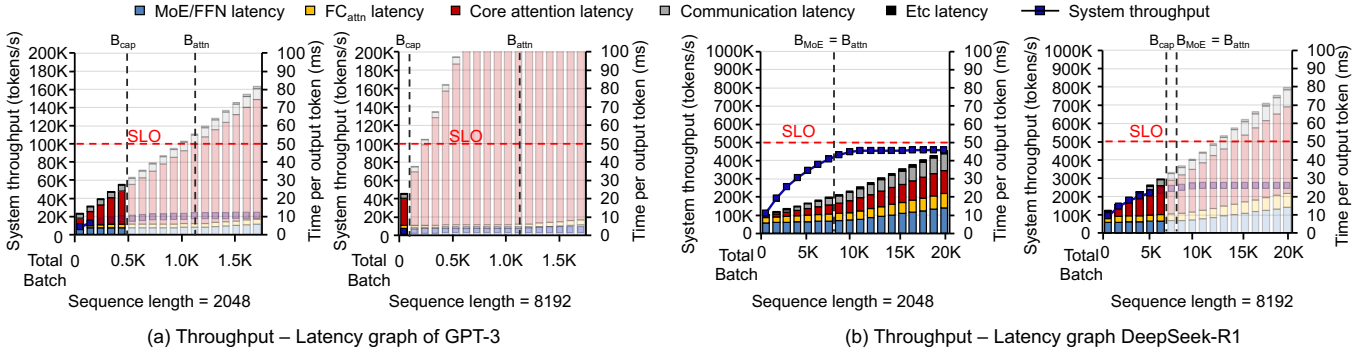


Fig. 9. Throughput-latency graph for the decode stages of GPT-3 and DeepSeek-R1. We assume a 32 B200 GPU system.

by the latency of each decoding stage and can be expressed as follows:

$$\text{TPOT}(B, L) = n_{\text{dec}} \cdot \left(\underbrace{\frac{M_{\text{attn}} \cdot \text{degDP} + M_{\text{MoE}}}{n_{\text{acc}} \cdot \text{BW}_{\text{Mem}}}}_{\text{model load lat.}} + \underbrace{T(B, L)}_{\text{additional lat.}} \right)$$

where both the first and second terms in the parentheses represent latencies for each decoder block: the first accounts for the latency to read model weights, and the second, $T(B, L)$, includes additional latency such as memory access time for the KV\$ and activations, communication overhead, and any remaining computation time. The additional latency term is a function of B and L .

As memory access time for the KV\$ and activations, along with communication time, is unavoidable while processing each decoder block, the minimum bound of this additional latency, $T_{\min}(B, L)$, is given by

$$T_{\min}(B, L) = B \cdot \left(\frac{M_{\text{KVcache}} \cdot L + M_{\text{act}}(L)}{n_{\text{acc}} \cdot \text{BW}_{\text{mem}}} \right) + \text{Comm}(B, L) \quad (12)$$

where $\text{Comm}(B, L)$ denotes the communication overhead between accelerators. Increasing B leads to larger KV\$ and activation sizes, thus increasing the minimum bound of TPOT. The theoretical maximum batch size, B_{SLO} , that satisfies the SLO time limit (TPOT_{SLO}) can be achieved under the minimum latency, and thus satisfies the following equation:

$$\text{TPOT}_{\text{SLO}} = n_{\text{dec}} \cdot \left(\frac{M_{\text{attn}} \cdot \text{degDP} + M_{\text{MoE}}}{n_{\text{acc}} \cdot \text{BW}_{\text{Mem}}} + T_{\min}(B_{\text{SLO}}, L) \right) \quad (13)$$

A batch size B greater than B_{SLO} can never satisfy the TPOT_{SLO} time limit, establishing an upper bound on the feasible batch size.

Observation-P6: While MoE tightens the batch size limit due to weight overhead, MLA complements this through its small KV\$ size.

MoE weights (M_{MoE}) are typically larger than the FFN weights in standard LLMs. As a result, MoE increases memory requirements for the model weights, reducing B_{cap} as less memory space remains for KV\$ (see Eq. 11). It also increases model load latency, which shortens the time available

for $T_{\min}(B_{\text{SLO}}, L)$, thereby reducing B_{SLO} . In contrast, the reduction of M_{KVcache} and M_{attn} by MLA enables storing KV\$ for more requests in main memory, thereby increasing B_{cap} . It also reduces the load time for M_{KVcache} and M_{attn} , allowing a higher B_{SLO} (see Eq. 12). Thus, as for batch size limits, MLA and MoE exhibit complementary effects.

VII. END-TO-END MODEL EXECUTION ANALYSIS

This section synthesizes our findings by analyzing the end-to-end execution of modern LLMs. We evaluate how the interplay between MLA, MoE, system scale, and interconnect bandwidth determines overall serving performance.

A. The Synergistic impact of MLA and MoE

LLMs using MLA and MoE achieve significantly higher throughput than conventional models. This is because MLA and MoE have a powerful synergistic relationship. MLA's highly-compressed KV\$ dramatically increases the memory capacity available for batching (B_{cap}). This, in turn, allows the system to form the large batches required to fully utilize the compute resources of the sparsely activated experts in MoE blocks, which would otherwise be constrained by memory.

Figure 9 illustrates this by comparing DeepSeek-R1 and GPT-3. For a sequence length of 8192, DeepSeek-R1's B_{cap} (7360) is nearly $60\times$ larger than GPT-3's (124). Consequently, DeepSeek-R1 can be configured with a batch size large enough to approach its ridge point $B_{\text{RP}} (= B_{\text{attn}})$, whereas GPT-3 becomes memory-capacity-limited long before its compute resources can be saturated.

Observation-P7: MLA and MoE are synergistic. MLA's KV\$ compression enables the large batch sizes, essential for MoE to achieve high *a.i.* and accelerator utilization.

B. Scaling the system out

While the MLA/MoE combination is powerful, memory capacity can still become a bottleneck for very long sequences. A natural response is to scale the system out by adding more accelerators (n_{acc}). However, this introduces a new trade-off. Increasing n_{acc} to raise the memory capacity limit (B_{cap}) also increases the batch size required to saturate the attention blocks (B_{attn}), as DP is distributed over more devices.

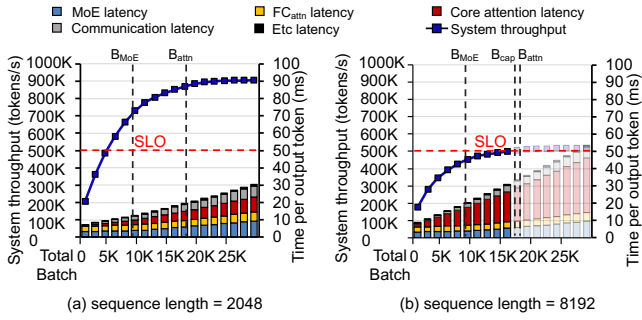


Fig. 10. System throughput and execution time ratio of operations in decode stage of DeepSeek-R1, varying batch sizes and sequence lengths. In this experiment, we assume a 64 B200 GPU system.

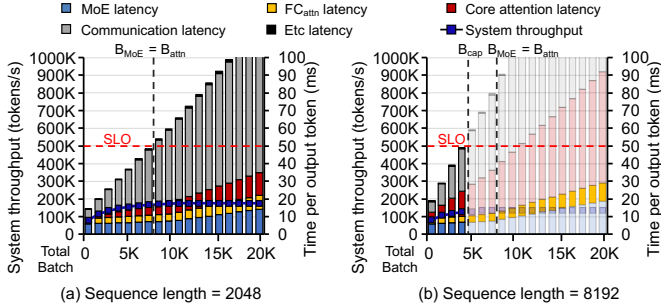


Fig. 11. System throughput and execution time ratio of decode stage of DeepSeek-R1 when using InfiniBand XDR (800Gb/s) among a group of GPUs (DGX) varying batch sizes and sequence length. We assume 32 B200 GPU system.

Figure 10 shows this effect when scaling from 32 to 64 GPUs. The increased memory capacity allows the system to reach the optimal batch size for MoE experts (B_{MoE}). However, because B_{attn} also doubles, the system may still fall short of the batch size needed to saturate the attention layers, particularly for very long sequences where core attention latency remains a significant factor.

Observation-P8: Scaling out a system for longer sequences creates a trade-off. While adding accelerators increases memory capacity, it raises the batch size required to keep them compute-bound, requiring careful system balancing.

C. The critical role of interconnect

The performance of a scaled-out MoE-based system is highly sensitive to interconnect bandwidth [10]. The all-to-all communication pattern, required to dispatch every token to its designated experts and then combine the results, creates dense network traffic that can easily become a bottleneck. As shown in Figure 11, moving from a high-bandwidth fabric like NVLink to a lower-bandwidth one like InfiniBand dramatically increases this communication overhead. Higher communication latency consumes a larger portion of the per-token time budget, which directly reduces the achievable batch size under a given SLO (B_{SLO}) and leads to underutilization. Thus, using a high bisection bandwidth interconnect is critical for efficient system deployment.

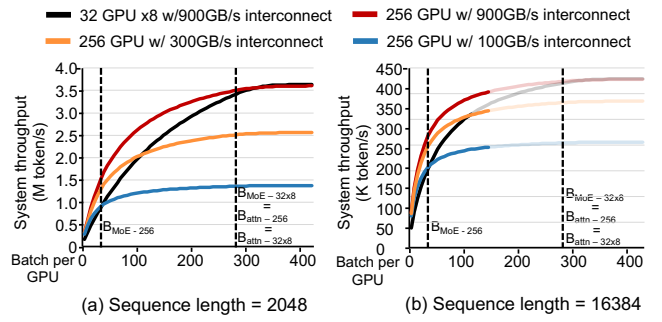


Fig. 12. Throughput comparison of **256 GPU** and **32 GPU** \times **8** systems of decode stage of DeepSeek-R1 when $L=2048$ and $L=16384$. 32GPUs are connected via 900 GB/s interconnect.

This sensitivity forces a critical deployment decision: using many small, tightly-coupled instances (*e.g.*, **32 GPU** \times **8**) versus one large, monolithic instance (*e.g.*, **256 GPU**). Since it is difficult to scale the number of accelerators while maintaining high bisection bandwidth, we vary the interconnect bandwidth of the **256 GPU** configuration to 900 GB/s, **300 GB/s**, and **100 GB/s**, which are equal to or lower than that of each **32 GPU** instance.

As Figure 12 shows, the optimal choice depends on the workload. For shorter sequences, multiple small instances are more cost-effective because communication is contained within high-bandwidth domains, and the memory overhead of replicating MoE weights is manageable. When $L=2048$ (Figure 12(a)), at the batch size B_{RP} where throughput is maximized, **32 GPU** \times **8** achieves equivalent throughput as **256 GPU** with 900 GB/s interconnect bandwidth. At this point, in **256 GPU**, each GPU is responsible for executing only one expert, but each expert processes 8 times more tokens than in **32 GPU** \times **8**. As the Op/B of experts in **256 GPU** falls in a compute-bound region, it results in higher latency. Thus, the latency of MoE blocks becomes similar in both systems.

For very long sequences (*e.g.*, $L=16384$ in Figure 12(b)), however, a single large instance is superior. The memory savings from storing the massive MoE weights only once by **256 GPU** frees up system-wide capacity for a larger B_{cap} , which is essential for handling the large KV\$, over **32 GPU** \times **8**. This leads to higher overall throughput, even if the large-scale interconnect has higher latency. For example, even with a reduced interconnect bandwidth of 300 GB/s, **256 GPU** delivers better throughput by reducing MoE execution latency.

Observation-P9: High-bandwidth interconnects are critical for MoE performance. The optimal system topology depends on the sequence length, which dictates the trade-off between the communication overhead of a large monolithic system and the memory-capacity overhead of replicating weights across many smaller systems.

VIII. CONCLUSION

Modern LLMs challenge the premise of specialized attention hardware. Architectural shifts to Multi-head Latent

Attention (MLA) and Mixture-of-Experts (MoE) move the performance bottleneck away from memory-bound attention. With layer reordering, MLA becomes a nearly compute-bound task well-suited for contemporary accelerators, diminishing the case for dedicated hardware. The new design challenge is balancing the complementary demands of MLA and MoE. MoE requires large batches for efficiency, creating memory pressure from its large weights. MLA alleviates this by drastically reducing KV cache size, which in turn enables the large batches required for efficient MoE execution on long sequences. These findings demand a new system design methodology. Data parallelism proves more effective than tensor parallelism for reordered MLA. Further, the all-to-all communication in MoE makes high-bandwidth interconnects critical for meeting latency SLOs and maximizing throughput in large-scale systems.

REFERENCES

- [1] A. Agrawal, N. Kedia, A. Panwar, J. Mohan, N. Kwatra, B. S. Gulavani, A. Tumanov, and R. Ramjee, "Taming throughput-latency tradeoff in LLM inference with sarathi-serve," in *Proceedings of the 18th USENIX Conference on Operating Systems Design and Implementation*, ser. OSDI'24. USA: USENIX Association, 2024. [Online]. Available: <https://dl.acm.org/doi/10.5555/3691938.3691945>
- [2] J. Ainslie, J. Lee-Thorp, M. de Jong, Y. Zemlyanskiy, F. Lebron, and S. Sanghai, "GQA: Training Generalized Multi-Query Transformer Models from Multi-Head Checkpoints," in *Proceedings of the 2023 Conference on Empirical Methods in Natural Language Processing*, Singapore, 2023, pp. 4895–4901. [Online]. Available: <https://aclanthology.org/2023.emnlp-main.298>
- [3] AMD, "AMD INSTINCT™ MI325X ACCELERATOR Leading-Edge, industry-standard accelerator module for generative AI, inference, training, and high performance computing." 2025. [Online]. Available: <https://www.amd.com/content/dam/amd/en/documents/instinct-tech-docs/product-briefs/instinct-mi325x-datasheet.pdf>
- [4] R. Y. Aminabadi, S. Rajbhandari, A. A. Awan, C. Li, D. Li, E. Zheng, O. Ruwase, S. Smith, M. Zhang, J. Rasley, and Y. He, "DeepSpeed-inference: enabling efficient inference of transformer models at unprecedented scale," in *Proceedings of the International Conference on High Performance Computing, Networking, Storage and Analysis*, 2022, pp. 1–15. [Online]. Available: <https://dl.acm.org/doi/abs/10.5555/3571885.3571946>
- [5] Y. Bai, X. Lv, J. Zhang, H. Lyu, J. Tang, Z. Huang, Z. Du, X. Liu, A. Zeng, L. Hou, Y. Dong, J. Tang, and J. Li, "LongBench: A Bilingual, Multitask Benchmark for Long Context Understanding," in *Proceedings of the 62nd Annual Meeting of the Association for Computational Linguistics (Volume 1: Long Papers)*. Bangkok, Thailand: Association for Computational Linguistics, Aug. 2024, pp. 3119–3137. [Online]. Available: <https://aclanthology.org/2024.acl-long.172/>
- [6] A. Bambhaniya, R. Raj, G. Jeong, S. Kundu, S. Srinivasan, S. Subramanian, M. Elavazhagan, M. Kumar, and T. Krishna, "Demystifying AI Platform Design for Distributed Inference of Next-Generation LLM models," 2025. [Online]. Available: <https://arxiv.org/abs/2406.01698>
- [7] T. Brown, B. Mann, N. Ryder, M. Subbiah, J. D. Kaplan, P. Dhariwal, A. Neelakantan, P. Shyam, G. Sastry, A. Askell, S. Agarwal, A. Herbert-Voss, G. Krueger, T. Henighan, R. Child, A. Ramesh, D. Ziegler, J. Wu, C. Winter, C. Hesse, M. Chen, E. Sigler, M. Litwin, S. Gray, B. Chess, J. Clark, C. Berner, S. McCandlish, A. Radford, I. Sutskever, and D. Amodei, "Language Models are Few-Shot Learners," in *Proceedings of the 34th International Conference on Neural Information Processing Systems*, 2020. [Online]. Available: https://proceedings.neurips.cc/paper_files/paper/2020/file/1457c0d6bfc4967418bfb8ac142f64a-Paper.pdf
- [8] J. Choi, J. Park, K. Kyung, N. S. Kim, and J. Ahn, "Unleashing the Potential of PIM: Accelerating Large Batched Inference of Transformer-Based Generative Models," *IEEE Computer Architecture Letters*, vol. 22, pp. 113–116, 2023. [Online]. Available: <https://doi.org/10.1109/LCA.2023.3305386>
- [9] D. Dai, C. Deng, C. Zhao, R. Xu, H. Gao, D. Chen, J. Li, W. Zeng, X. Yu, Y. Wu, Z. Xie, Y. Li, P. Huang, F. Luo, C. Ruan, Z. Sui, and W. Liang, "DeepSeekMoE: Towards Ultimate Expert Specialization in Mixture-of-Experts Language Models," in *Proceedings of the 62nd Annual Meeting of the Association for Computational Linguistics (Volume 1: Long Papers)*, 2024, pp. 1280–1297. [Online]. Available: <https://aclanthology.org/2024.acl-long.70/>
- [10] W. Dally and B. Towles, *Principles and Practices of Interconnection Networks*. Morgan Kaufmann, 2004.
- [11] DeepSeek-AI, D. Guo, D. Yang, H. Zhang, J. Song, R. Zhang, R. Xu, Q. Zhu, S. Ma, P. Wang, X. Bi, X. Zhang, X. Yu, Y. Wu, Z. F. Wu, Z. Gou, Z. Shao, Z. Li, Z. Gao, A. Liu, B. Xue, B. Wang, B. Wu, B. Feng, C. Lu, C. Zhao, C. Deng, C. Zhang, C. Ruan, D. Dai, D. Chen, D. Ji, E. Li, F. Lin, F. Dai, F. Luo, G. Hao, G. Chen, G. Li, H. Zhang, H. Bao, H. Xu, H. Wang, H. Ding, H. Xin, H. Gao, H. Qu, H. Li, J. Guo, J. Li, J. Wang, J. Chen, J. Yuan, J. Qiu, J. Li, J. L. Cai, J. Ni, J. Liang, J. Chen, K. Dong, K. Hu, K. Gao, K. Guan, K. Huang, K. Yu, L. Wang, L. Zhang, L. Zhao, L. Wang, L. Zhang, L. Xu, L. Xia, M. Zhang, M. Zhang, M. Tang, M. Li, M. Wang, M. Li, N. Tian, P. Huang, P. Zhang, Q. Wang, Q. Chen, Q. Du, R. Ge, R. Zhang, R. Pan, R. Wang, R. J. Chen, R. L. Jin, R. Chen, S. Lu, S. Zhou, S. Chen, S. Ye, S. Wang, S. Yu, S. Zhou, S. Pan, S. S. Li, S. Zhou, S. Wu, S. Ye, T. Yun, T. Pei, T. Sun, T. Wang, W. Zeng, W. Zhao, W. Liu, W. Liang, W. Gao, W. Yu, W. Zhang, W. L. Xiao, W. An, X. Liu, X. Wang, X. Chen, X. Nie, X. Cheng, X. Liu, X. Xie, X. Liu, X. Yang, X. Li, X. Su, X. Lin, X. Q. Li, X. Jin, X. Shen, X. Chen, X. Sun, X. Wang, X. Song, X. Zhou, X. Wang, X. Shan, Y. K. Li, Y. Q. Wang, Y. X. Wei, Y. Zhang, Y. Xu, Y. Li, Y. Zhao, Y. Sun, Y. Wang, Y. Yu, Y. Zhang, Y. Shi, Y. Xiong, Y. He, Y. Piao, Y. Wang, Y. Tan, Y. Ma, Y. Liu, Y. Guo, Y. Ou, Y. Wang, Y. Gong, Y. Zou, Y. He, Y. Xiong, Y. Luo, Y. You, Y. Liu, Y. Zhou, Y. X. Zhu, Y. Xu, Y. Huang, Y. Li, Y. Zheng, Y. Zhu, Y. Ma, Y. Tang, Y. Zha, Y. Yan, Z. Z. Ren, Z. Ren, Z. Sha, Z. Fu, Z. Xu, Z. Xie, Z. Zhang, Z. Hao, Z. Ma, Z. Yan, Z. Wu, Z. Gu, Z. Zhu, Z. Liu, Z. Li, Z. Xie, Z. Song, Z. Pan, Z. Huang, Z. Xu, Z. Zhang, and Z. Zhang, "DeepSeek-R1: Incentivizing Reasoning Capability in LLMs via Reinforcement Learning," 2025. [Online]. Available: <https://arxiv.org/abs/2501.12948>
- [12] DeepSeek-AI, A. Liu, B. Feng, B. Xue, B. Wang, B. Wu, C. Lu, C. Zhao, C. Deng, C. Zhang, C. Ruan, D. Dai, D. Guo, D. Yang, D. Chen, D. Ji, E. Li, F. Lin, F. Dai, F. Luo, G. Hao, G. Chen, G. Li, H. Zhang, H. Bao, H. Xu, H. Wang, H. Zhang, H. Ding, H. Xin, H. Gao, H. Li, H. Qu, J. Cai, J. Liang, J. Guo, J. Ni, J. Li, J. Wang, J. Chen, J. Chen, J. Yuan, J. Qiu, J. Li, J. Song, K. Dong, K. Hu, K. Gao, K. Guan, K. Huang, K. Yu, L. Wang, L. Zhang, L. Xu, L. Xia, L. Zhao, L. Wang, L. Zhang, M. Li, M. Wang, M. Zhang, M. Zhang, M. Tang, M. Li, N. Tian, P. Huang, P. Wang, P. Zhang, Q. Wang, Q. Zhu, Q. Chen, Q. Du, R. Chen, R. Jin, R. Ge, R. Zhang, R. Pan, R. Wang, R. Xu, R. Zhang, R. Chen, S. Li, S. Lu, S. Zhou, S. Chen, S. Wu, S. Ye, S. Ye, S. Ma, S. Wang, S. Zhou, S. Yu, S. Zhou, S. Pan, T. Wang, T. Yun, T. Pei, T. Sun, W. Xiao, W. Zeng, W. Zhao, W. An, W. Liu, W. Liang, W. Gao, W. Yu, W. Zhang, X. Li, X. Jin, X. Wang, X. Bi, X. Liu, X. Wang, X. Shen, X. Chen, X. Zhang, X. Chen, X. Nie, X. Sun, X. Wang, X. Cheng, X. Liu, X. Xie, X. Liu, X. Yu, X. Song, X. Shan, X. Zhou, X. Yang, X. Li, X. Su, X. Lin, Y. Li, Y. Wang, Y. Wei, Y. Zhu, Y. Zhang, Y. Xu, Y. Xu, Y. Huang, Y. Li, Y. Zhao, Y. Sun, Y. Li, Y. Wang, Y. Yu, Y. Zheng, Y. Zhang, Y. Shi, Y. Xiong, Y. He, Y. Tang, Y. Piao, Y. Wang, Y. Tan, Y. Ma, Y. Liu, Y. Guo, Y. Wu, Y. Ou, Y. Zhu, Y. Wang, Y. Gong, Y. Zou, Y. He, Y. Zha, Y. Xiong, Y. Ma, Y. Yan, Y. Luo, Y. You, Y. Liu, Y. Zhou, Z. Wu, Z. Ren, Z. Ren, Z. Sha, Z. Fu, Z. Xu, Z. Huang, Z. Zhang, Z. Xie, Z. Zhang, Z. Hao, Z. Gou, Z. Ma, Z. Yan, Z. Shao, Z. Xu, Z. Wu, Z. Zhang, Z. Li, Z. Gu, Z. Zhu, Z. Liu, Z. Li, Z. Xie, Z. Song, Z. Gao, and Z. Pan, "DeepSeek-V3 Technical Report," 2024. [Online]. Available: <https://arxiv.org/abs/2412.19437>
- [13] K. Du, B. Wang, C. Zhang, Y. Cheng, Q. Lan, H. Sang, Y. Cheng, J. Yao, X. Liu, Y. Qiao, I. Stoica, and J. Jiang, "PrefillOnly: An Inference Engine for Prefill-only Workloads in Large Language Model Applications," 2025. [Online]. Available: <https://arxiv.org/abs/2505.07203>
- [14] A. Elmeleegy, S. Raj, B. Slechta, and V. Mehta, "Demystifying AI Inference Deployments for Trillion Parameter Large Language Models," [Online]. Available: <https://developer.nvidia.com/blog/demystifying-ai-inference-deployments-for-trillion-parameter-large-language-models/>

- [15] W. Fedus, B. Zoph, and N. Shazeer, "Switch Transformers: Scaling to Trillion Parameter Models with Simple and Efficient Sparsity," *Journal of Machine Learning Research*, vol. 23, no. 120, pp. 1–39, 2022. [Online]. Available: <http://jmlr.org/papers/v23/21-0998.html>
- [16] J. Feng, Y. Huang, R. Zhang, S. Liang, M. Yan, and J. Wu, "WindServe: Efficient Phase-Disaggregated LLM Serving with Stream-based Dynamic Scheduling," in *ISCA*, 2025. [Online]. Available: <https://dl.acm.org/doi/10.1145/3695053.3730999>
- [17] D. Foley and J. Danskin, "Ultra-Performance Pascal GPU and NVLink Interconnect," *IEEE Micro*, vol. 37, no. 2, pp. 7–17, 2017. [Online]. Available: <https://dl.acm.org/doi/abs/10.1109/MM.2017.37>
- [18] P. Grun, "Introduction to Infiniband for End Users," *White paper, InfiniBand Trade Association*, vol. 55, 2010. [Online]. Available: https://network.nvidia.com/pdf/whitepapers/Intro_to_IB_for_End_Users.pdf
- [19] A. Gu and T. Dao, "Mamba: Linear-Time Sequence Modeling with Selective State Spaces," 2024. [Online]. Available: <https://arxiv.org/abs/2312.00752>
- [20] G. Heo, S. Lee, J. Cho, H. Choi, S. Lee, H. Ham, G. Kim, D. Mahajan, and J. Park, "NeuPIMs: NPU-PIM Heterogeneous Acceleration for Batched LLM Inference," in *ASPLOS*, 2024, p. 722–737. [Online]. Available: <https://doi.org/10.1145/3620666.3651380>
- [21] Y. Huang, Y. Cheng, A. Bapna, O. Firat, D. Chen, M. Chen, H. Lee, J. Ngiam, Q. V. Le, Y. Wu, and Z. Chen, "GPipe: Efficient Training of Giant Neural Networks using Pipeline Parallelism," in *Advances in Neural Information Processing Systems* 32, 2019, pp. 103–112. [Online]. Available: <https://proceedings.neurips.cc/paper/2019/hash/093f65e080a295f8076b1c5f722a46aa2-Abstract.html>
- [22] A. Q. Jiang, A. Sablayrolles, A. Roux, A. Mensch, B. Savary, C. Bamford, D. S. Chaplot, D. de las Casas, E. B. Hanna, F. Bressand, G. Lengyel, G. Bour, G. Lample, L. R. Lavaud, L. Saulnier, M.-A. Lachaux, P. Stock, S. Subramanian, S. Yang, S. Antoniak, T. L. Scao, T. Gervet, T. Lavril, T. Wang, T. Lacroix, and W. E. Sayed, "Mixtral of Experts," 2024. [Online]. Available: <https://arxiv.org/abs/2401.04088>
- [23] S. L. Jiashi Li, "FlashMLA: Efficient MLA decoding kernels," 2025. [Online]. Available: <https://github.com/deepseek-ai/FlashMLA>
- [24] J. Kaplan, S. McCandlish, T. Henighan, T. B. Brown, B. Chess, R. Child, S. Gray, A. Radford, J. Wu, and D. Amodei, "Scaling Laws for Neural Language Models," 2020. [Online]. Available: <https://arxiv.org/abs/2001.08361>
- [25] H. Kwon, K. Koo, J. Kim, W. Lee, M. Lee, H. Lee, Y. Jung, J. Park, Y. Song, B. Yang, H. Choi, G. Kim, J. Won, W. Shin, C. Kim, G. Shin, Y. Kwon, I. Kim, E. Lim, J. Kim, and J. Choi, "LoL-PIM: Long-Context LLM Decoding with Scalable DRAM-PIM System," 2025. [Online]. Available: <https://arxiv.org/abs/2412.20166>
- [26] D. Lepikhin, H. Lee, Y. Xu, D. Chen, O. Firat, Y. Huang, M. Krikun, N. Shazeer, and Z. Chen, "GShard: Scaling Giant Models with Conditional Computation and Automatic Sharding," in *International Conference on Learning Representations*, 2021. [Online]. Available: <https://openreview.net/forum?id=qrwe7XHTmYb>
- [27] A. Liu, B. Feng, B. Wang, B. Wang, B. Liu, C. Zhao, C. Deng, C. Ruan, D. Dai, D. Guo, D. Yang, D. Chen, D. Ji, E. Li, F. Lin, F. Luo, G. Hao, G. Chen, G. Li, H. Zhang, H. Xu, H. Yang, H. Zhang, H. Ding, H. Xin, H. Gao, H. Li, H. Qu, J. Cai, J. Liang, J. Guo, J. Ni, J. Li, J. Chen, J. Yuan, J. Qiu, J. Song, K. Dong, K. Gao, K. Guan, L. Wang, L. Zhang, L. Xu, L. Xia, L. Zhao, L. Zhang, M. Li, M. Wang, M. Zhang, M. Zhang, M. Tang, M. Li, N. Tian, P. Huang, P. Wang, P. Zhang, Q. Zhu, Q. Chen, Q. Du, R. Chen, R. Jin, R. Ge, R. Pan, R. Xu, R. Chen, S. Li, S. Lu, S. Zhou, S. Chen, S. Wu, S. Ye, S. Ma, S. Wang, S. Zhou, S. Yu, S. Zhou, S. Zheng, T. Wang, T. Pei, T. Yuan, T. Sun, W. Xiao, W. Zeng, W. An, W. Liu, W. Liang, W. Gao, W. Zhang, X. Li, X. Jin, X. Wang, X. Bi, X. Liu, X. Wang, X. Shen, X. Chen, X. Chen, X. Nie, X. Sun, X. Wang, X. Liu, X. Xie, X. Yu, X. Song, X. Zhou, X. Yang, X. Lu, X. Su, Y. Wu, Y. Li, Y. Wei, Y. Zhu, Y. Xu, Y. Huang, Y. Li, Y. Zhao, Y. Sun, Y. Li, Y. Wang, Y. Zheng, Y. Zhang, Y. Xiong, Y. Zhao, Y. He, Y. Tang, Y. Piao, Y. Dong, Y. Tan, Y. Liu, Y. Wang, Y. Guo, Y. Zhu, Y. Wang, Y. Zou, Y. Zha, Y. Ma, Y. Yan, Y. You, Y. Liu, Z. Ren, Z. Ren, Z. Sha, Z. Fu, Z. Huang, Z. Zhang, Z. Xie, Z. Hao, Z. Shao, Z. Wen, Z. Xu, Z. Zhang, Z. Li, Z. Wang, Z. Gu, Z. Li, and Z. Xie, "DeepSeek-V2: A Strong, Economical, and Efficient Mixture-of-Experts Language Model," 2024. [Online]. Available: <https://arxiv.org/abs/2405.04434>
- [28] C. Liu, H. Liu, D. Chen, Y. Huang, Y. Zhang, W. Xiao, X. Liao, and H. Jin, "HeterRAG: Heterogeneous Processing-in-Memory Acceleration for Retrieval-augmented Generation," in *ISCA*, 2025, p. 884–898. [Online]. Available: <https://doi.org/10.1145/3695053.3731089>
- [29] A. Meta, "The llama 4 herd: The beginning of a new era of natively multimodal ai innovation," 2025. [Online]. Available: <https://ai.meta.com/blog/llama-4-multimodal-intelligence/>
- [30] S. Nie, F. Zhu, Z. You, X. Zhang, J. Ou, J. Hu, J. Zhou, Y. Lin, J.-R. Wen, and C. Li, "Large Language Diffusion Models," 2025. [Online]. Available: <https://arxiv.org/abs/2502.09992>
- [31] NVIDIA, "NVIDIA V100 GPU," 2017. [Online]. Available: <https://images.nvidia.com/content/volta-architecture/pdf/volta-architecture-whitepaper.pdf>
- [32] NVIDIA, "NVIDIA A100 GPU," 2020. [Online]. Available: <https://www.nvidia.com/content/dam/en-zz/Solutions/Data-Center/a100/pdf/nvidia-a100-datasheet-nvidia-us-2188504-web.pdf>
- [33] NVIDIA, "NVIDIA GB200 NVL72," 2024. [Online]. Available: <https://www.nvidia.com/en-us/data-center/gb200-nvl72/>
- [34] NVIDIA, "NVIDIA H100 GPU," 2024. [Online]. Available: <https://resources.nvidia.com/en-us-hopper-architecture/nvidia-tensor-core-gpu-datasheet>
- [35] Nvidia, "Dynamo," 2025. [Online]. Available: <https://github.com/ai-dynamo/dynamo?tab=readme-ov-file>
- [36] NVIDIA, "NVIDIA Blackwell Architecture Technical Brief," 2025. [Online]. Available: <https://resources.nvidia.com/en-us-blackwell-architecture>
- [37] NVIDIA, "NVIDIA Quantum-X800 InfiniBand Switches," 2025. [Online]. Available: <https://nvdam.widen.net/s/nfdzskhmnc/infiniband-datasheet-quantum-family-3231555>
- [38] OpenAI, J. Achiam, S. Adler, S. Agarwal, L. Ahmad, I. Akkaya, F. L. Aleman, D. Almeida, J. Altenschmidt, S. Altman, S. Anadkat, R. Avila, I. Babuschkin, S. Balaji, V. Balcom, P. Baltescu, H. Bao, M. Bavarian, J. Belgum, I. Bello, J. Berdine, G. Bernadett-Shapiro, C. Berner, L. Bogdonoff, O. Boiko, M. Boyd, A.-L. Brakman, G. Brockman, T. Brooks, M. Brundage, K. Button, T. Cai, R. Campbell, A. Cann, B. Carey, C. Carlson, R. Carmichael, B. Chan, C. Chang, F. Chantzis, D. Chen, S. Chen, R. Chen, J. Chen, M. Chen, B. Chess, C. Cho, C. Chu, H. W. Chung, D. Cummings, J. Currier, Y. Dai, C. Decareaux, T. Degry, N. Deutsch, D. Deville, A. Dhar, D. Dohan, S. Dowling, S. Dunning, A. Ecoffet, A. Eleti, T. Eloundou, D. Farhi, L. Fedus, N. Felix, S. P. Fishman, J. Forte, I. Fulford, L. Gao, E. Georges, C. Gibson, V. Goel, T. Gogineni, G. Goh, R. Gontijo-Lopes, J. Gordon, M. Grafstein, S. Gray, R. Greene, J. Gross, S. S. Gu, Y. Guo, C. Hallacy, J. Han, J. Harris, Y. He, M. Heaton, J. Heidecke, C. Hesse, A. Hickey, W. Hickey, P. Hoeschele, B. Houghton, K. Hsu, S. Hu, X. Hu, J. Huizinga, S. Jain, S. Jain, J. Jang, A. Jiang, R. Jiang, H. Jin, D. Jin, S. Jomoto, B. Jonn, H. Jun, T. Kaftan, Łukasz Kaiser, A. Kamali, I. Kanitscheider, N. S. Keskar, T. Khan, L. Kilpatrick, J. W. Kim, C. Kim, Y. Kim, J. H. Kirchner, J. Kiros, M. Knight, D. Kokotajlo, Łukasz Kondruciuk, A. Kondrich, A. Konstantinidis, K. Kosic, G. Krueger, V. Kuo, M. Lampe, I. Lan, T. Lee, J. Leung, D. Levy, C. M. Li, R. Lim, M. Lin, S. Lin, M. Litwin, T. Lopez, R. Lowe, P. Lue, A. Makanju, K. Malfacini, S. Manning, T. Markov, Y. Markovski, B. Martin, K. Mayer, A. Mayne, B. McGrew, S. M. McKinney, C. McLeavey, P. McMillan, J. McNeil, D. Medina, A. Mehta, J. Menick, L. Metz, A. Mishchenko, P. Mishkin, V. Monaco, E. Morikawa, D. Mossing, T. Mu, M. Murati, O. Murk, D. Mély, A. Nair, R. Nakano, R. Nayak, A. Neelakantan, R. Ngo, H. Noh, L. Ouyang, C. O’Keefe, J. Pachocki, A. Paino, J. Palermo, A. Pantuliano, G. Parascandolo, J. Parish, E. Parparita, A. Passos, M. Pavlov, A. Peng, A. Perelman, F. de Avila Belbute Peres, M. Petrov, H. P. de Oliveira Pinto, Michael, Pokorny, M. Pokrass, V. H. Pong, T. Powell, A. Power, B. Power, E. Proehl, R. Puri, A. Radford, J. Rae, A. Ramesh, C. Raymond, F. Real, K. Rimbach, C. Ross, B. Rotsted, H. Roussez, N. Ryder, M. Saltarelli, T. Sanders, S. Santurkar, G. Sastry, H. Schmidt, D. Schnurr, J. Schulman, D. Selsam, K. Sheppard, T. Sherbakov, J. Shieh, S. Shoker, P. Shyam, S. Sidor, E. Sigler, M. Simens, J. Sitkin, K. Slama, I. Sohl, B. Sokolowsky, Y. Song, N. Staudacher, F. P. Such, N. Summers, I. Sutskever, J. Tang, N. Tezak, M. B. Thompson, P. Tillet, A. Tootoonchian, E. Tseng, P. Tuggle, N. Turley, J. Tworek, J. F. C. Uribe, A. Vallone, A. Vijayvergiya, C. Voss, C. Wainwright, J. J. Wang, A. Wang, B. Wang, J. Ward, J. Wei, C. Weinmann, A. Welihinda, P. Welinder, J. Weng, L. Weng, M. Wiethoff, D. Willner, C. Winter, S. Wolrich, H. Wong, L. Workman, S. Wu, J. Wu, M. Wu, K. Xiao, T. Xu, S. Yoo, K. Yu, Q. Yuan, W. Zaremba, R. Zellers, C. Zhang, M. Zhang, S. Zhao, T. Zheng, J. Zhuang, W. Zhuk, and B. Zoph, "GPT-4 Technical Report," 2024. [Online]. Available: <https://arxiv.org/abs/2303.08774>

- [39] J. Park, J. Choi, K. Kyung, M. J. Kim, Y. Kwon, N. S. Kim, and J. Ahn, "AttAcc! Unleashing the Power of PIM for Batched Transformer-based Generative Model Inference," in *ASPLOS*, Volume 2, 2024, p. 103–119. [Online]. Available: <https://doi.org/10.1145/3620665.3640422>
- [40] P. Patel, E. Choukse, C. Zhang, A. Shah, I. Goiri, S. Maleki, and R. Bianchini, "Splitwise: Efficient Generative LLM Inference Using Phase Splitting," in *ISCA*, 2024. [Online]. Available: <https://doi.org/10.1109/ISCA59077.2024.00019>
- [41] R. Pope, S. Douglas, A. Chowdhery, J. Devlin, J. Bradbury, J. Heek, K. Xiao, S. Agrawal, and J. Dean, "Efficiently Scaling Transformer Inference," in *Efficiently Scaling Transformer Inference*, 2023. [Online]. Available: https://proceedings.mlsys.org/paper_files/paper/2023/hash/c4be71ab8d24cdfb45e3d06dbfca2780-Abstract-mlsys2023.html
- [42] L. Poutievski, O. Mashayekhi, J. Ong, A. Singh, M. Tariq, R. Wang, J. Zhang, V. Beauregard, P. Conner, S. Gribble, R. Kapoor, S. Kratzer, N. Li, H. Liu, K. Nagaraj, J. Ornstein, S. Sawhney, R. Urata, L. Vicisano, K. Yasumura, S. Zhang, J. Zhou, and A. Vahdat, "Jupiter Evolving: Transforming Google's Datacenter Network via Optical Circuit Switches and Software-Defined Networking," in *Proceedings of ACM SIGCOMM 2022*, 2022, p. 66–85. [Online]. Available: <https://doi.org/10.1145/3544216.3544265>
- [43] S. Rajbhandari, C. Li, Z. Yao, M. Zhang, R. Y. Aminabadi, A. A. Awan, J. Rasley, and Y. He, "DeepSpeed-MoE: Advancing Mixture-of-Experts Inference and Training to Power Next-Generation AI Scale," in *Proceedings of the 39th International Conference on Machine Learning*, ser. Proceedings of Machine Learning Research, vol. 162, 2022, pp. 18 332–18 346. [Online]. Available: <https://proceedings.mlr.press/v162/rajbhandari22a.html>
- [44] SCALE-SNU, "LLMSimulator — GitHub Repository," 2025. [Online]. Available: <https://github.com/scale-snu/LLMSimulator>
- [45] N. Shazeer, "Fast Transformer Decoding: One Write-Head is All You Need," 2019. [Online]. Available: <https://arxiv.org/abs/1911.02150>
- [46] N. Shazeer, "GLU Variants Improve Transformer," 2020. [Online]. Available: <https://arxiv.org/abs/2002.05202>
- [47] N. Shazeer, A. Mirhoseini, K. Maziarz, A. Davis, Q. Le, G. Hinton, and J. Dean, "Outrageously Large Neural Networks: The Sparsely-Gated Mixture-of-Experts Layer," 2017. [Online]. Available: <https://arxiv.org/abs/1701.06538>
- [48] M. Shoenybi, M. Patwary, R. Puri, P. LeGresley, J. Casper, and B. Catanzaro, "Megatron-LM: Training Multi-Billion Parameter Language Models Using Model Parallelism," 2020. [Online]. Available: <https://arxiv.org/abs/1909.08053>
- [49] J. Su, Y. Lu, S. Pan, A. Murtadha, B. Wen, and Y. Liu, "RoFormer: Enhanced Transformer with Rotary Position Embedding," 2023. [Online]. Available: <https://arxiv.org/abs/2104.09864>
- [50] A. Vahdat, "Ironwood: The First Google TPU for the Age of Inference," 2025. [Online]. Available: <https://blog.google/products/google-cloud/ironwood-tpu-age-of-inference/>
- [51] A. Vahdat and M. Lohmeyer, "Enabling next-generation AI workloads: Announcing TPU v5p and AI Hypercomputer," 2023. [Online]. Available: <https://cloud.google.com/blog/products/ai-machine-learning/introducing-cloud-tpu-v5p-and-ai-hypercomputer?hl=en>
- [52] A. Vaswani, N. Shazeer, N. Parmar, J. Uszkoreit, L. Jones, A. N. Gomez, L. u. Kaiser, and I. Polosukhin, "Attention is All you Need," in *Proceedings of the 31st International Conference on Neural Information Processing Systems*, 2017. [Online]. Available: <https://dl.acm.org/doi/10.5555/3295222.3295349>
- [53] J. Wei, X. Wang, D. Schuurmans, M. Bosma, B. Ichter, F. Xia, E. Chi, Q. Le, and D. Zhou, "Chain-of-Thought Prompting Elicits Reasoning in Large Language Models," 2023. [Online]. Available: <https://arxiv.org/abs/2201.11903>
- [54] S. Williams, A. Waterman, and D. Patterson, "Roofline: an insightful visual performance model for multicore architectures," *Commun. ACM*, vol. 52, p. 65–76, 2009. [Online]. Available: <https://doi.org/10.1145/1498765.1498785>
- [55] xAI, "grok1," 2024. [Online]. Available: <https://github.com/xai-org/grok-1>
- [56] S. Yun, K. Kyung, J. Cho, J. Choi, J. Kim, B. Kim, S. Lee, K. Sohn, and J. Ahn, "Duplex: A Device for Large Language Models with Mixture of Experts, Grouped Query Attention, and Continuous Batching," in *MICRO*, 2024, pp. 1429–1443. [Online]. Available: <https://ieeexplore.ieee.org/abstract/document/10764531>
- [57] S. Zhang, N. Zheng, H. Lin, Z. Jiang, W. Bao, C. Jiang, Q. Hou, W. Cui, S. Zheng, L.-W. Chang, Q. Chen, and X. Liu, "COMET: Fine-grained Computation-communication Overlapping for Mixture-of-Experts," in *Proceedings of Machine Learning and Systems*, 2025. [Online]. Available: <https://openreview.net/forum?id=fGgQSS5VW09>
- [58] Y. Zhang, R. Sun, Y. Chen, T. Pfister, R. Zhang, and S. Arik, "Chain of Agents: Large Language Models Collaborating on Long-Context Tasks," 2024. [Online]. Available: <https://arxiv.org/abs/2406.02818>
- [59] Y. Zhong, S. Liu, J. Chen, J. Hu, Y. Zhu, X. Liu, X. Jin, and H. Zhang, "DistServe: Disaggregating Prefill and Decoding for Goodput-optimized Large Language Model Serving," in *18th USENIX Symposium on Operating Systems Design and Implementation (OSDI 24)*. USENIX Association, 2024, pp. 193–210. [Online]. Available: <https://www.usenix.org/conference/osdi24/presentation/zhong-yinmin>

APPENDIX

TABLE IV
SYMBOLS USED THROUGHOUT THIS PAPER, THEIR DESCRIPTIONS, AND THE EXEMPLAR PARAMETERS USED IN DEEPSEEK-R1 [11]

| Term | Description | DeepSeek-R1 | Term | Description | DeepSeek-R1 |
|---------------------|------------------------------------|-------------|---|------------------------------------|--|
| TP/DP/EP | Tensor / Data / Expert Parallelism | - | O_t | Context output | - |
| $deg_{TP/DP/EP}$ | TP / DP / EP degree | - | U_t | Final attention output / FFN input | - |
| B | Batch size | - | H_t | FFN output / Decoder block input | - |
| L | Sequence length | - | RP_{device} | Ridge point of device | - |
| n_{dec} | Decoder blocks | 61 | Q, K, V | Query, Key, Value | - |
| d_{emb} | Embedding dimension | 7168 | W_Q, W_K, W_V | Weight for Q, K, V generation | - |
| n_{hd} | Number of heads | 128 | W_{attn_out} | Out projection weight in attention | (16384, 7168) |
| d_{hd} | Head dimension | 128 | W_{gate}, W_{up} | Weight for gate/up in FFN | (7168, 18432) |
| d_{dec} | Decompressed Q, KV dimension | 16384 | W_{down} | Weight for down in FFN | (18432, 7168) |
| d_{Qco}, d_{KVco} | Compressed Q, KV dimension | 1536, 512 | W_{route} | MoE route weight | (7168, 256) |
| d_{RoPE} | Rotary PE dimension | 64 | $W_{exp_n, gate}, W_{exp_n, up}, W_{exp_n, down}$ | MoE up/down projection weights | (7168, 2048), (7168, 2048), (2048, 7168) |
| d_{MoE} | MoE dimension | 2048 | W_{CQ}, W_{CKV} | Q comp / KV compression | (7168, 1536), (7168, 512) |
| n_k | Top-k experts | 8 | W_{DQ} | Q decompression weight | (1536, 16384) |
| n_e | Number of experts | 256 | W_{DK}, W_{DV} | K, V decompression weights | (512, 16384) |
| Q_{NoPE} | Query vector (No RoPE) | (1, 16384) | W_{RQ} | RoPE Q weight | (1536, 8192) |
| Q_{RoPE} | Query after RoPE | (1, 8192) | W_{RK} | RoPE K weight | (7168, 64) |
| K_{RoPE} | Key vector for RoPE | (1, 64) | C_Q | Latent Q (compressed) | - |
| S_{RoPE} | Score output with RoPE | - | C_{KV} | Latent KV (compressed) | - |
| S_{NoPE} | Score output without RoPE | - | n_{acc} | Number of accelerators | - |
| S_t | Final score output | - | - | - | - |